Check for updates

Sonochemical synthesis of polyoxometalate-stabilized gold nanoparticles for point-of-care determination of acetaminophen levels: preclinical study in an animal model†

Tahereh Rohani Bastami, [iD] *[ab] Abolphazl Ghaedi,[c] Scott G. Mitchell, [iD] [d]
Aida Javadian-Saraf[e] and Mohammad Karimi[f]

The aim of this study is the accurate and rapid detection of acetaminophen (AP) for point-of-care (POC) clinical diagnosis. Acetaminophen overdose causes acute liver failure and currently there is a lack of rapid quantitative detection methods for this drug in the emergency room. Here, low-frequency sonication (20 kHz) in the presence of phosphomolybdic acid (PMo_{12}) was used to reduce Au^{3+} to Au^0 and stabilize the resulting spherical Au^0 nanoparticles (herein AuNPs). These AuNPs@PMo_{12} were used as nano-probes for the selective detection of acetaminophen in the presence of other commercial drugs. The optical sensing method we describe is based on the aggregation of AuNPs@PMo_{12} in the presence of acetaminophen, which produces a red-shift in the absorption spectrum of the AuNPs@PMo_{12}, which is characterised by a color change from red to purple that is visible to the naked eye. Furthermore, the quantitative determination of acetaminophen concentrations can be carried out using the eyedropper function in Microsoft's PowerPoint or open access ImageJ software, using RGB (red, green, and blue) values. To prove the feasibility of this novel nanosensor, the concentration of acetaminophen was measured in over-the-counter pharmaceutical tablets and in serum samples taken from mice. This simple sensing approach offers high stability, selectivity, rapid detection time, and cost saving compared to other detection methods, which therefore opens the way for the development of quantitative POC acetaminophen detection using polyoxometalate-stabilized metal nanoparticles.

Introduction

Acetaminophen (AP), also known as paracetamol, is one of the most commonly used medicinal compounds in the world.[1] According to the Food and Drug Administration (FDA) guidelines, taking up to 4 grams of AP per 24 hours is safe.[2] Although the toxic dose of the drug that can cause liver failure is usually greater than 15 grams in a single dose, studies have reported that lower doses may also cause acute liver injury and liver

[a]Department of Chemical Engineering, Quchan University of Technology, Quchan 94771-67335, Iran. E-mail: t.rohani@qiet.ac.ir; tahereh.rohani@gmail.com

[b]Research and Technology Center of Biomolecules, Faculty of Science, Ferdowsi University of Mashhad, Mashhad, 9177948974, Iran

[c]Department of Chemical Engineering, Quchan University of Technology, Quchan 94771-67335, Iran

[d]Instituto de Ciencia de Materiales de Aragón (ICMA), Consejo Superior de Investigaciones Científicas (CSIC)-Universidad de Zaragoza and CIBER-BBN, C/ Pedro Cerbuna 12, 50009 Zaragoza, Spain

[e]School of Engineering, University of British Columbia, Kelowna, BC, V1V 1V7, Canada

[f]Department of Emergency Medicine, Faculty of Medicine, Ahvaz Jundishapur University, Ahvaz, Iran

† Electronic supplementary information (ESI) available. See DOI: 10.1039/d0ra00931h

failure.[3] The only clinically effective antidote against AP-induced liver injury is NAC (*N*-acetylcysteine), which has the greatest effect when administered within the first 8 hours after overdose.[4] Currently, the Rumack–Matthew nomogram (plot of serum AP concentration *vs.* time after acute ingestion) is used to determine patients who require NAC and patients who have serum AP levels below the treatment line will not need treatment.[5]

This study aimed to develop a sensitive, rapid, low cost, and green nanosensor for the quantitative determination of toxic levels of AP in blood serum in the early hours after ingestion. Recently, the detection of AP has received much attention from the analytical chemistry field where a variety of analytical methods have been developed, including titrimetric methods,[6] high-performance liquid chromatography (HPLC),[7] spectrophotometry,[8] chemiluminescence,[9] and electrochemical analysis.[10] One promising technology for clinical and personalized point-of-care (POC) diagnostics is colorimetric sensing of target analytes. Because of their unique optical properties, plasmonic nano-materials, such as gold nanoparticles (AuNPs) have been introduced into colorimetric sensing systems to provide high selectivity and sensitivity in different biosensing applications.[11,12]

Polyoxometalates (POMs) are an important class of inorganic compounds that are well-known due to the broad range of applications in biochemistry[13] and sensing.[14] They can be applied as both reducing and stabilizing agents in aqueous solutions at room temperature.[15] Furthermore, the ability of the multi-electron redox reaction of POMs make them particularly useful for the synthesis of noble metal nanoparticles.[16–18]

In recent years, it has become increasingly clear that there is a critical need for green-chemistry-type synthetic routes to new materials.[19] In 2009, Zhang *et al.*[20] introduced the one-pot, aqueous preparation of AuNPs with mixed-valence polyoxometalates. Liu *et al.*[21] presented the method to synthesize AuNP@POM composites on graphene. To improve the electrocatalytic activities electrodes for the reduction of H_2O_2, Suo *et al.*[22] synthesized core–shell POM-stabilized AuNPs as part of a composite assembly with graphene oxide.

To date, the most common technique used to obtain POM-stabilized metal(0) NPs involves using UV irradiation.[23] However, few studies have investigated alternative approaches for the reduction of the metal precursor. Sonochemistry has emerged as one of the more promising and scalable methods to obtain metal NPs,[24] whereby the chemical effects of ultrasonic irradiation can be tailored due to the acoustic cavitation phenomenon. When the liquid is exposed to ultrasonic irradiation, air bubbles are generated and then collapse, leading to the release of the ultrasonic energy during a very short time. The extremely high local temperature (>5000 K), pressure (>20 MPa) and very high cooling rates (>10^{10} K s^{-1}) are suitable conditions for reducing metal ions and polyoxometalates.[25–27]

The present research explores, for the first time, the eco-friendly and practical synthesis of polyoxometalate-stabilized gold nanoparticles (AuNPs@PMo$_{12}$) using ultrasonication. Sono-synthesized samples were kept at room temperature and remained stable for more than three months. The synthesized AuNPs@PMo$_{12}$ were used as optical nanosensors for the highly selective naked-eye detection and quantitative determination of acetaminophen (AP). Our results show that AP molecules induced a strong and selective aggregation of the AuNPs@PMo$_{12}$ which can be detected by naked eye and verified by conventional UV-vis spectroscopy. It is worth mentioning that a combination of quantitative and qualitative approaches was used in this research project. To achieve the optimization of the AuNPs@PMo$_{12}$ nano-hybrids for sensing application, acoustic intensity, reaction temperature, and Au : POM ratios were investigated. This project provided an important opportunity to advance the understanding of the detection of AP in mice serum by using AuNPs@PMo$_{12}$ nano-hybrids.

Experimental

Materials

All reagents were purchased and used without further purification. Phosphomolybdic acid, $H_3PMo_{12}O_{40}$, (PMo$_{12}$), sodium hydroxide and hydrochloric acid (37%) were purchased from Merck Company and were used without further treatment. 1-Propanol (C_3H_7OH), was purchased from Sigma-Aldrich. HAuCl$_4$ solution (0.1 M, 3.4% w/v) was freshly purchased from

Kimia next Company, Iran. Acetaminophen ($C_8H_9NO_2$), methadone ($C_{21}H_{27}NO$), methylphenidate ($C_{14}H_{19}NO_2$), and tramadol ($C_{16}H_{25}NO_2$) were obtained from Temad Pharmaceutical Company in Iran. The physicochemical properties of AP are shown in Table S1†.[28] Mili-Q water was used with minimum resistivity of 18.2 MΩ cm^{-1}.

Ultrasonication synthesis of AuNPs@PMo$_{12}$ nano-hybrid (US method)

The ultrasonic synthesis (US method) of AuNPs@PMo$_{12}$ was carried out using ultrasonic equipment at various temperatures for 30 min with different ratios of Au : POM (1 : 2, 1 : 1, 2 : 1). In this experiment, the effect of acoustic intensity, Au : POM ratio, and reaction temperature on colorimetric detection of AP have been investigated. The resulting liquid in every synthesis was ready for the characterization and detection of AP. The synthesis process was as follows: Briefly, 16.5 mL of 1 mM HAuCl$_4$ solution was added to 33 mL of 1 mM PMo$_{12}$ and stirred at room temperature. After magnetic stirring, the resulting solution poured into 100 mL Dewar cell, and 1.2 mL of propanol added into this solution. The resulting solution was exposed to ultrasonication through an ultrasonic horn (20 kHz, Branson Digital Sonifier-USA, W-450 D). Various acoustic amplitudes (40%, 50%, and 60%) were used to provide different acoustic power of 20 W, 25 W, and 29 W, respectively. After sono-reaction, the aqueous solution turned wine red, indicating gold nanoparticle formation. Finally, the prepared AuNPs@PMo$_{12}$ nano-hybrid was kept at room temperature and remained stable for more than three months.

One reaction was conducted as follows to determine the effect of ultrasonic irradiation on the reduction of PMo$_{12}$: 33 mL of 1 mM PMo$_{12}$ solution was added to 16.5 mL of distilled water and stirred at room temperature. After magnetic stirring, the resulting solution poured into 100 mL Dewar cell, and 1.2 mL of propanol added into the solution. This solution was sonicated using an ultrasonic horn (20 kHz, Branson Digital Sonifier-USA, W-450D). The acoustic amplitude of 50% was applied to deliver acoustic power of 25 W. After 30 min sonication, the aqueous solution turned pale green (Scheme 1).

Synthesis of AuNPs@PMo$_{12}$ nano-hybrid without ultrasonic irradiation (UV-method)

In this experiment, UV-lamp was used instead of ultrasonic irradiation but, no change in the color of the solution was observed under the same condition of US method up to 100 min. So, it is concluded that no product was obtained under the same condition. However, in the less volume of chemicals, AuNPs@PMo$_{12}$ nano-hybrids were produced according to the following procedure:[29] 5 mL of an aqueous solution of PMo$_{12}$ (0.001 M), 2.5 mL HAuCl$_4$ (0.001 M), and 2 mL 1-propanol were placed into a beaker. The final solution was then irradiated by UV light (125 W high-pressure mercury vapor lamp) under magnetic stirring. The solution color changed from colorless to wine red, confirming the formation of AuNPs. The time of reaction fixed at 35 min. Finally, the prepared AuNPs@PMo$_{12}$ was kept at room temperature and remained stable for less than
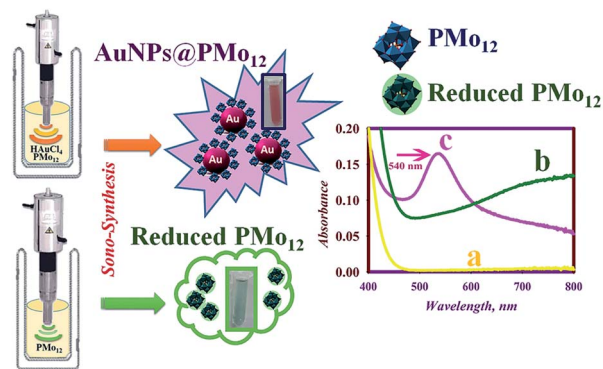
Scheme 1 The synthetic strategy for AuNPs@PMo$_{12}$ showing the preparation and reduction of PMo$_{12}$ under ultrasonic irradiation ((a) PMo$_{12}$O$_{40}$$^{3-}$ solution, (b) reduced PMo$_{12}$O$_{40}$$^{4-}$, (c) AuNP@PMo$_{12}$) (synthesis condition: intensity = 26 W cm^{-2}, $T = 37 \pm 1$ °C, Au : POM ratio (1 : 2)).

one week. The same results reported by other kinds of literature.[29]

Detection of acetaminophen (AP)

Colorimetric detection of AP was performed by using AuNPs@PMo$_{12}$ as a nano-probe. Briefly, 0.9 mL of an aqueous solution with different concentrations of AP (from 0 to 120 mg L^{-1}) were added separately into 0.9 mL of AuNPs@PMo$_{12}$ solution. After mixing the above solution, the change of color of the solution was investigated by UV-visible spectroscopy, and photographs were recorded with a digital camera. The high-angle annular dark field-scanning transmission electron microscopy (HAADF-STEM) was used to measure the diameters and morphological changes of AuNPs@PMo$_{12}$ in the presence of AP, which confirms the aggregation of AuNPs@PMo$_{12}$ induced by AP.

Quantitative determination of acetaminophen by the RGB value

The extraordinary development of smartphones and tablets has made a great opportunity for researchers to develop their methods by using smartphones as a chemical detector. These highly reliable portable devices which have a digital camera and internal microprocessor for image processing, reduce using external computers and expensive devices. In this work, to obtain the calibration curve by analyzing the average RGB (red, green, and blue) value, the pictures of different concentrations of AP samples were taken. To verify the reliability of the smartphone as a chemical detector, we used two methods for analyzing the color changes. The RGB values were obtained by eyedropper function in the Microsoft Office PowerPoint 2016 software and ImageJ software. The quantitative determination was made by transforming the RGB value to AP concentration. The trend of RGB values of ImageJ is consistent with the eyedropper.

Acetaminophen assay in mice serum

After a therapeutic dose, AP is changed to pharmacologically inactive glucuronide (AP-gluc, 52–57% of urinary metabolites) and sulfate (AP sulfate, 30–44%) conjugates, with a minor fraction being oxidized to a reactive metabolite NAPQI (5–10%). Less than 5% of AP is excreted unchanged.[30] At supratherapeutic doses of AP (more than 4 g per day), sulfation approach becomes saturated, while glucuronidation and oxidation increase, and a smaller amount is excreted unchanged. After a single highly toxic dose of AP, glucuronidation becomes saturated and high proportions of the drug are eliminated unchanged (~10%) and are oxidized to NAPQI (>15%).[30]

The serum acetaminophen (AP) concentration is the basis for diagnosis and treatment. As the dose of AP increase the amount of unchanged AP in the serum increased. So, the measurement of unchanged AP in the serum depends on the amount of AP adiminstration. The Rumack–Matthew nomogram uses the serum acetaminophen concentration, in relation to the time after ingestion, to assess potential hepatotoxicity after a single, acute ingestion of acetaminophen.

To establish the toxic serum AP level in the blood, 2 g kg^{-1} of AP was fed to mice (100 mice) *via* the feeding tube. Two hours after AP ingestion, blood samples were obtained from mice. Serum AP levels were recorded at three levels based on the color change of nanosensor and baseline liver tests. The mice were divided into three groups based on the serum AP level determined by the nanosensor. The first group (>100 μg mL^{-1}), the second group (25–100 μg mL^{-1}) and the third group (<25 μg mL^{-1}) were considered as high risk, medium risk, and low-risk groups, respectively. Blood samples were obtained five h again after AP ingestion in mice. Changes in liver enzymes in each group were compared to baseline status.

To evaluate the accuracy of the nanosensor in another way, the researcher prepared three hundred solutions with different AP concentrations and recorded the number of the container and the concentration of dissolved AP in the container. The second researcher, who was unaware of the research protocol, was asked to use the nanosensor solution to detect the AP level in each test tube at one of the levels of (>100 μg mL^{-1}), (25–100 μg mL^{-1}) or (<25 μg mL^{-1}). In the end, the levels determined by the nanosensor were compared with the actual concentration of the solution. This experimental study was conducted under approval of Ethics Committee of Ahvaz Jundishapur University of Medical Sciences. All animal experiments carried out in accordance with the European Communities Council Directive of 24 November 1986 (86/609/EEC) to minimize damage to the animals.

Characterization and apparatus

The crystal structure of the resulting product was carried out on a Bruker D8-Focus using Cu Kα radiation ($\lambda = 0.154\ 056$ nm) in the range of $2\theta = 10$–$80°$. High-angle annular dark field-scanning transmission electron microscopy (HAADF-STEM) images were collected using a Tecnai S-Twin 30, 300 keV, GIF-TRIDIEM. Energy-dispersive X-ray spectroscopy (EDS) data were obtained on the same instrument. The UV-vis spectra were recorded by an Evolution 201 spectrophotometer (Thermo Fisher Scientific). IR spectra were recorded on a Thermo Nicolet

Avatar-370-FTIR spectrometer (Thermo Fisher scientific, United states). Zeta-potential measurement performed by Zeta Compact (CAD instrumentation, France). Dynamic light scattering (DLS) was conducted on Vasco Particle Size Analyzer (Cordouan Technologies). Atomic force microscopy (AFM) images were obtained with a NAMA AFM nanotechnology system corporation (NATSYCO) machine. Electrochemical analysis were conducted using a µ-Autolab type III electrochemical workstation. The analysis were performed at room temperature using a conventional three-electrode set-up. Platinum wire (Azar Electrod Co.) served as the counter electrode and Ag/AgCl as the reference electrode (Azar Electrod Co.). Experiments under ultrasonic irradiation were performed with equipment operating at 20 kHz (Branson Digital sonifier, Model W-450 D). It includes a double cylindrical jacket with a volume of 100 mL to control of temperature. The 20 kHz ultrasonic irradiations were emitted from the tip with a diameter of 1.1 cm which is located at the end of the horn.

Determination of acoustic intensity

Acoustic power and intensity were determined by a colorimetric method.[25,31] Since the ultrasonic irradiation of a liquid generates heat, recording the temperatures as a function of time causes to the acoustic power calculation by the following equation (eqn (1)):

$$P = mC_p\left(\frac{dT}{dt}\right) \qquad (1)$$

where m is the mass of the sonicated liquid (g), C_p is the specific heat of medium, and dT/dt is the temperature rise per second.[25] Various amplitudes (40%, 50% and 60%) were used to deliver different acoustic power of 20 W, 25 W and 29 W, and different intensity of 21 W cm^{-2}, 26 W cm^{-2}, 30.5 W cm^{-2} respectively.
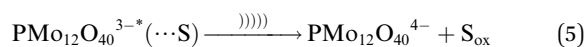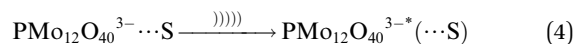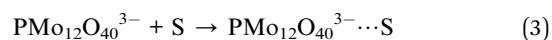
Results and discussions

### Sonochemical synthesis of AuNPs@PMo$_{12}$ nano-hybrid

The sono-reduction process of PMo$_{12}$ and Au ions was carried out using ultrasonic irradiation (US) which is shown in Scheme 1. Before US irradiation of PMo$_{12}$ solution, no significant absorption band was observed in the visible region (curve (a) in Scheme 1). After sonication of the PMo$_{12}$ solution, a broad absorption band centered at 750 nm was obtained and the solution became pale green (curve (b) in Scheme 1).[28] The observation of a new metal-to-metal intervalence charge transfer (IVCT) band confirmed the electron transfer between the organic substrate (1-propanol) and heteropolyanions (PMo$_{12}$O$_{40}^{3-}$) which produced the reduced form of PMo$_{12}$ (PMo$_{12}$O$_{40}^{4-}$) (pale green solution). Furthermore, the sonication of PMo$_{12}$ solution in the presence of Au ions led to the synthesis of AuNPs@PMo$_{12}$ (pink solution, curve c in Scheme 1). In water media, PMo$_{12}$ dissociated as the following equation (eqn (2)):

$$H_3PMo_{12}O_{40} \xrightarrow{H_2O} PMo_{12}O_{40}^{3-} + 3H^+ \qquad (2)$$
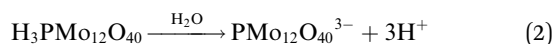
Before US irradiation the pH of the reactants in water media was measured at pH 3.5 ± 0.5. It is suggested that an association between the PMo$_{12}$O$_{40}^{3-}$ and 1-propanol (S) occurred under US irradiation in aqueous media. The sono-reduction of the PMo$_{12}$ is shown as follows (eqn (3)–(5)):[32,33]
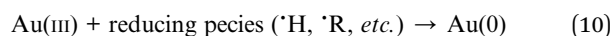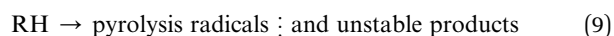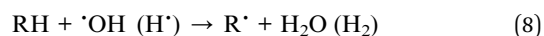
$$PMo_{12}O_{40}^{3-} + S \rightarrow PMo_{12}O_{40}^{3-}\cdots S \qquad (3)$$

$$PMo_{12}O_{40}^{3-}\cdots S \xrightarrow{\;))))))\;} PMo_{12}O_{40}^{3-*}(\cdots S) \qquad (4)$$

$$PMo_{12}O_{40}^{3-*}(\cdots S) \xrightarrow{\;))))))\;} PMo_{12}O_{40}^{4-} + S_{ox} \qquad (5)$$

Electrons accumulated on the PMo$_{12}$O$_{40}^{4-}$ can be withdrawn by different electron acceptors (eqn (6)):[34]

$$PMo_{12}O_{40}^{4-} + oxidant \xrightarrow{\;))))))\;} PMo_{12}O_{40}^{3-}, etc. \qquad (6)$$
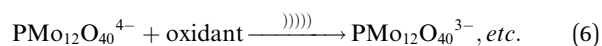
In eqn (6), *etc.* refers to reducing form of oxidant, O$_2^-$ and H$_2$O due to reduction of O$_2$ and H$^+$. The reduced form of PMo$_{12}$ is a strong reducing agent that leads to the reduction of metal ions into their corresponding metal nanoparticles. In the case of gold ion, the following reaction occurs (eqn (7)):[35]

$$3PMo_{12}O_{40}^{4-} + Au^{3+} \xrightarrow{\;))))))\;} 3PMo_{12}O_{40}^{3-}\cdots Au^o + 3H^+ \qquad (7)$$
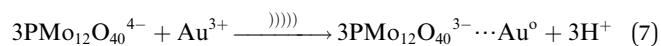
According to Okitsu *et al.*[26] under ultrasonic waves, localized hotspots with a high temperature are produced due to the rapid collapse of cavitation bubbles. Under such conditions, the homolysis of water molecules gives rise to highly reactive H$^·$ and OH$^·$ radicals.[26,34] The sono-reduction of Au(III) in the presence of an organic additive (1-propanol) can occure via the following reactions[26] (eqn (8)–(10)):

$$RH + {}^·OH\ (H^·) \rightarrow R^· + H_2O\ (H_2) \qquad (8)$$

$$RH \rightarrow pyrolysis\ radicals\ \vdots\ and\ unstable\ products \qquad (9)$$

$$Au(III) + reducing\ pecies\ ({}^·H,\ {}^·R,\ etc.) \rightarrow Au(0) \qquad (10)$$

where RH is an organic additive. Reactions (8) and (9) show the sonochemical formation of the reducing radicals and reductants: (1) $^·$H is created by sonolysis of water, (2) $^·$R and H$_2$ are created from the abstraction reaction of RH with $^·$OH or $^·$H, and (3) pyrolysis of RH and water led to the pyrolysis radicals and unstable products. Finally, the generated organic radicals can reduce the target substrate in solution, which in this instance are Au(III) metal ions, through further complex reaction steps.[26] Consequently, the reduction of PMo$_{12}$ and gold ions are also accelerated under such ultrasonic irradiation.

According to the reactions (8)–(10) the rate of Au(III) reduction stongly depends on the concentration of ther primary and secondary reducing radicals. However, the acoustic intensity also affects other reaction parameters, such as temperature and pressure inside the collapsing cavitation bubbles, the size, number and distribution of bubbles, and the effect of 1-propanol on bubble temperature, secondary radical formation, and so forth.[26]

In the case of synthesis procedure, the effect of various parameters like sonication time, ultrasonic amplitude (intensity), reaction temperature, and Au: POM ratio on the synthesis of AuNPs@PMo$_{12}$ nano-hybrids and their sensor activity has also been studied. Scheme 1 represents the synthetic strategy for AuNPs@PMo$_{12}$ preparation and reduction of PMo$_{12}$ under ultrasonic irradiation.

Characterization of AuNPs@PMo$_{12}$ nano-hybrid

After the reduction of Au^{3+} ions with PMo$_{12}$ as a reducing and stabilizing agent, the AuNPs@PMo$_{12}$ nano-hybrids were characterized by UV-visible, FT-IR, high angle annular dark-field scanning transmission electron microscopy (HAADF-STEM), Energy Dispersive X-ray Spectroscopy (EDS), zeta potential, Atomic Force Microscope (AFM), electrochemical measurements, and Dynamic Light Scattering (DLS), respectively.

In Fig. 1a, XRD pattern of the AuNPs@PMo$_{12}$ nano-hybrid reveals the face-centered cubic (FCC) structure of the Au crystals with distinguished peaks in 38.1°, 44.3°, 64.5° and 77.5°, which correspond to the (111), (200), (220) and (311) crystal faces of metallic gold nanoparticle in accordance with JCPDS-04-0784.[36,37] As shown in Fig. 1a, the peak corresponding to the (111) planes of Au is much sharper in comparison with the other planes of Au, which approves the predominant orientation of Au (111). The average particle size calculated from the Au (111) peak according to the Scherrer equation was 22 nm. Also, no obvious diffraction peaks were observed related to the crystallized POMs or Mo oxides.[38] Therefore, it can be assumed that the POMs are adsorbed onto the surface of AuNPs with no agglomeration.[39]

FTIR spectroscopy was performed to verify the formation of AuNPs@PMo$_{12}$ nano-hybrids. Fig. 1b shows the spectra and infrared transmission frequencies of PMo$_{12}$ and AuNPs@PMo$_{12}$. The characteristic peaks of PMo$_{12}$ at 1060 cm^{-1} and 966 cm^{-1} are due to ν_{as} (P–O) and ν_{as} (Mo–O$_d$), which appear in AuNPs@PMo$_{12}$ at 1080 cm^{-1} with a shoulder in 1033 cm^{-1}.[38] This blue shift (shorter wavelength) approves the interaction between PMo$_{12}$ and the surface of Au.[40] The peak at 876 cm^{-1} is due to the vibration of (Mo–O$_b$–Mo), a stretch that disappears in the AuNPs@PMo$_{12}$ sample.[38] The peak around 796 cm^{-1} is attributed to the vibration of (Mo–O$_c$–Mo) and shows a red-shift (increase wavelength) in the AuNPs@PMo$_{12}$ at 619 cm^{-1}. These results suggest an interaction between PMo$_{12}$ and Au via (Mo–O$_c$–Mo) group. Table S2† shows the most

important IR vibrations for PMo$_{12}$ and AuNPs@PMo$_{12}$ nano-hybrid.

DLS analysis was used to measure the size distribution and hydrodynamic diameter of AuNPs@PMo$_{12}$ in water. DLS data agrees well with the average particle size calculated from the Scherrer equation. The average size of AuNPs@PMo$_{12}$ is found to be 19.8 ± 1.7 nm (synthesis condition: intensity = 26 W cm^{-2}, $T = 37 \pm 1$ °C, Au : POM ratio (1 : 2)). A polydispersity index (PDI) of 0.17 was obtained indicating monodispersed AuNPs.

ζ-Potential measurements were used to characterize the surface potential of an as-prepared AuNPs@PMo$_{12}$ colloidal solution. The measurement is crucial for studying the dispersion manners of the nanoparticles in a liquid media. The higher the ζ potential leads to a more stable suspension.[41,42] The average ζ potential of suspensions was −2 mV. According to these results, the surface of NPs negatively charged due to the coating of PMo$_{12}$ polyanions on the Au surface. Also, the results show high colloidal stability (for several months), and no precipitation was observed during this time.

The electrostatic repulsions between charged particles cause more dispersed particles and less coagulation.[42] In our case, it seems that the ζ-potential is not sufficiently high to produce high colloidal stability of nanoparticles in the medium. It is proposed that the hydrogen bonding between OH groups in water and adsorbed PMo$_{12}$ molecules on the surface of AuNPs is responsible for the observed stability. Besides, the greater stability of dispersion could be due to the solvation of adsorbed PMo$_{12}$ molecules onto the surface of AuNPs.[41] The FTIR results confirm this assumption. Also, results show that the AuNPs@PMo$_{12}$ nano-hybrids which were synthesized under ultrasonic irradiation have higher stability than those synthesized with more conventional UV irradiation methods. There are two crucial factors about the PMo$_{12}$ coating onto AuNPs surface: (1) increasing of mass transfer owing to shock waves action and microjets and (2) surface corrosion due to the collapse of a bubble near the surface.[39] Therefore, the predominant factor determines the amount of PMo$_{12}$ coating on the surface. The former leads to increasing of PMo$_{12}$ coating onto the surface of
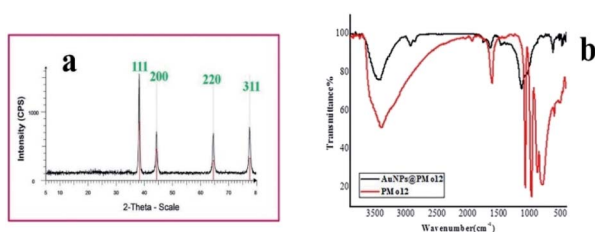

Fig. 1 (a) XRD pattern of AuNPs@PMo$_{12}$ nano-hybrid, (b) FT-IR spectra of PMo$_{12}$ and AuNPs@PMo$_{12}$ nano-hybrid (synthesis condition: intensity = 26 W cm^{-2}, $T = 37 \pm 1$ °C, Au : POM ratio (1 : 2)).
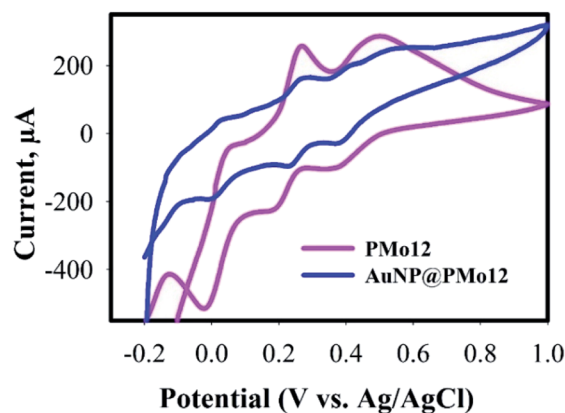

Fig. 2 Cyclic voltammograms (CVs) of AuNP@PMo$_{12}$ and pure PMo$_{12}$ in 50% (v/v) water–DMF solution containing 1 M H$_2$SO$_4$ (synthesis condition: intensity = 26 W cm^{-2}, $T = 37 \pm 1$ °C, Au : POM ratio (1 : 2)).

AuNPs, and the later causes the desorption of coated PMo_{12} from the surface of AuNPs. In our case, it is assumed that the balance between the two parameters has occurred.

The existence of PMo_{12} in the AuNPs@PMo_{12} was further verified by electrochemical measurements. It should be noted that PMo_{12} can undergo a multi-electron reversible redox process without losing its integrity. The cyclic voltammograms (CVs) of PMo_{12} and AuNPs@PMo_{12} in 50% v/v water: DMF solution containing 1 M H_2SO_4 as an electrolyte are shown in Fig. 2. By comparing the CVs of PMo_{12} and AuNPs@PMo_{12}, it can be concluded that voltammetric peaks at *ca.* −0.02, 0.18 and 0.4 V (*vs.* Ag/AgCl) in AuNPs@PMo_{12} electrode should be originated from the characteristic redox behavior of PMo_{12}. Furthermore, PMo_{12} is adsorbed on Au during the synthesis of the AuNPs@PMo_{12}.

Scanning electron microscopy (SEM) and HAADF-STEM images were effectively applied to investigate the morphology of AuNPs@PMo_{12} (Fig. 3, 4 and 5). All figures show truncated tetrahedral and hexagonal shapes. Furthermore, the rod-like structure was observed by increasing of acoustic power. According to the results, the size of nanoparticles and length of nanorods increased with increasing of acoustic power. The average size of AuNPs@PMo_{12} nanoparticles was obtained 20 nm, 24 nm, and 34 nm for 21 W cm^{-2}, 26 W cm^{-2}, and 30.5 W cm^{-2} respectively. Also, the average length of the rod-like structure was obtained around 85 nm and 106 nm for 26 W cm^{-2} and 30.5 W cm^{-2}, respectively. We propose that ultrasonic irradiation under these conditions led to corrosion of surface and desorption of capping agents (PMo_{12}) from the surface of nanoparticle due to the collapse of cavitation. For this reason, the larger size of nanoparticles can be obtained under high-intensity ultrasonic waves.
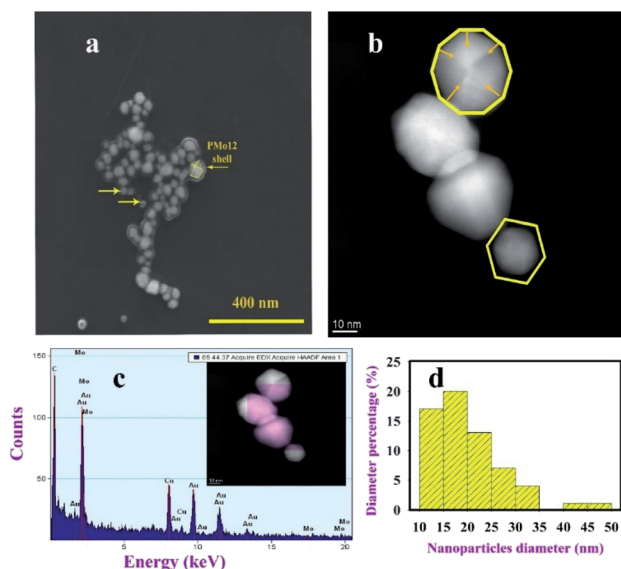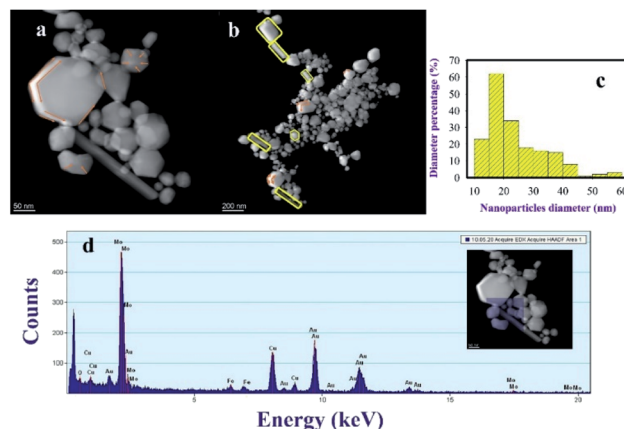

Fig. 4 (a and b) HAADF-STEM images of AuNPs@PMo_{12} nano-hybrid, (c) particle size distribution histogram showing average diameter of 24 nm ± 9 nm (from *ca.* 190 NPs), and (d) EDS analysis and corresponding HAADF-STEM image (blue part) synthesized by 26 W cm^{-2} (synthesis condition: $T = 37 \pm 1\,°C$, Au : POM ratio (1 : 2)).

Furthermore, in the growth process *via* a diffusion-controlled crystal, each crystal is surrounded by a diffusion sphere.[31] It is suggested that ultrasonic waves enhance the mass transfer and diffusion of precursors from the bulk into the diffusion sphere, so the facets along the more active axis should be rapidly growing and led to the generation of faceted and 1D structure especially by increasing of acoustic intensity. Another key factor of the growth process is the diffusion sphere thickness, which is decreased by ultrasonic irradiation, and this phenomenon led to an increase in flux diffusion and rapid growth along the active axis.[31]

The chemical composition analysis of AuNPs@PMo_{12} was determined using EDS analysis (Fig. 3 and 4). A cross-sectional EDS line scan profiles extracted from the HAADF-STEM images confirmed the coverage of Mo in the immediate area surrounding the AuNPs, suggesting they are from the PMo_{12} structure. The Cu peaks are the signal detected from the SEM grid.

Optimization of acetaminophen (AP) detection conditions

To optimize the AuNPs@PMo_{12} for AP sensing, parameters such as the temperature of the reaction, acoustic intensity, Au : POM ratio, and sample pH value were investigated.
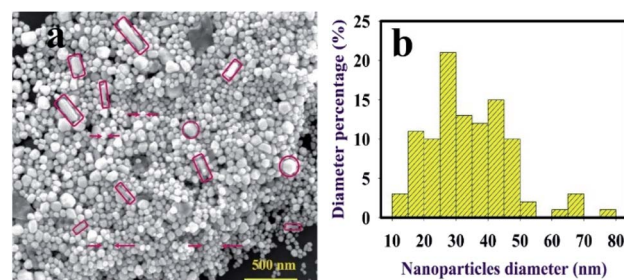

Fig. 3 (a) SEM image, (b) HAADF-STEM image, (c) EDS analysis and corresponding HAADF-STEM image (purple part on image) of AuNPs@PMo_{12} nano-hybrid synthesized by 21 W cm^{-2}, and (d) particle size distribution histogram showing average diameter of 20 nm ± 7 nm (from *ca.* 90 NPs) (synthesis condition: $T = 37 \pm 1\,°C$, Au : POM ratio (1 : 2)).

Fig. 5 (a) SEM image of AuNPs@PMo_{12} nano-hybrid synthesized by 30.5 W cm^{-2}, and (b) particle size distribution histogram showing the average diameter of 34 nm ± 12 nm (from *ca.* 100 NPs) (synthesis condition: $T = 37 \pm 1\,°C$, Au : POM ratio (1 : 2)).

Effect of reaction temperature

In the sonochemical reaction, the effect of temperature was investigated in 27 ± 1 °C, 37 ± 1 °C, and 47 ± 1 °C (Fig. 6). The conditions of sonochemical reaction were as follows: intensity, 26 W cm^{-2}; and 1 : 2 Au : POM ratio. To investigate the effect of reaction temperature, AP aqueous solution (0.9 mL) was added to the AuNPs@PMo$_{12}$ solution (0.9 mL). After 5 seconds the color of the solution was changed from light pink to dark pink (30 mg L^{-1}), and purple (70 mg L^{-1}). According to the results (Table S3†), the SPR peak of AuNPs@PMo$_{12}$ is red-shifted by increasing temperature, which confirms the increase of particle size of AuNPs nanoparticles by increasing temperature. These results reveal that the maximum of SPR peak red-shifted by increasing AP concentration from 30 mg L^{-1} to 70 mg L^{-1}. According to the results, the red-shift of the SPR peak confirmed that the NPs aggregated upon addition of AP.[43] Based on the obtained results, the temperature of 37 ± 1 °C was selected as the optimum temperature.

Effect of acoustic intensity

The amplitude of sonication was changed in the range of 40–60% (corresponding to an acoustic intensity of 21 W cm^{-2}, 26 W cm^{-2}, and 30.5 W cm^{-2}, respectively), to better understand the effect of acoustic intensity on the AuNPs@PMo$_{12}$ synthesis. The UV-visible absorbance spectra of AuNPs@PMo$_{12}$ in different acoustic amplitudes and intensities are shown in Fig. 7. In this case, the conditions of sonochemical reaction were as follows; temperature; 37 ± 1 °C and Au : POM ratio of 1 : 2. The SPR peak of AuNPs@PMo$_{12}$ is slightly red-shifted from 537 nm to 541 nm and 550 nm for 21 W cm^{-2}, 26 W cm^{-2}, and 30.5 W cm^{-2}, respectively (Fig. 7 and Table S4†). This result confirms increasing acoustic intensity leads to increase in the size of particles.[37] According to results, the change of color for 26 W cm^{-2} was significant. We therefore selected an amplitude of 50%, which corresponds to an intensity of 26 W cm^{-2} for other experiments.
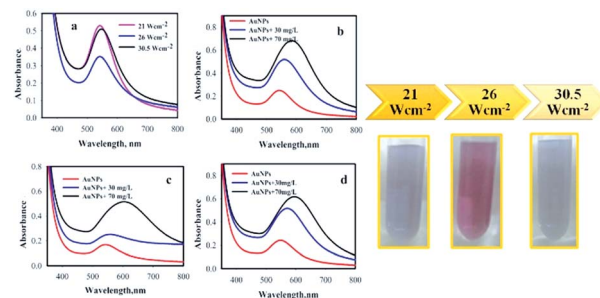

Fig. 7 Effect of different acoustic intensity on (a) SPR peak of AuNPs@PMo$_{12}$, (b) upon addition of AP (21 W cm^{-2}), (c) (26 W cm^{-2}), and (d) (30.5 W cm^{-2}). (Pictures show visual color change of AuNPs@PMo$_{12}$ after addition of AP (30 mg L^{-1}) (synthesis condition: $T = 37 \pm 1$ °C, Au : POM ratio (1 : 2)).

Effect of Au : POM ratio

The UV-visible absorbance spectra of AuNPs@PMo$_{12}$ in different Au : POM ratio is shown in Fig. 8. This condition of sonochemical reactions was as follows; temperature, 37 ± 1 °C; and intensity, 26 W cm^{-2}. Comparing three different ratios, the SPR peaks for Au : POM ratio of 1 : 2 shows more red-shifted by different concentration of AP (Fig. 8 and Table S5†). According to results, the change of color for Au : POM ratio (1 : 2) was significant, so this ratio was selected for all further experiments.

Effect of sample pH value

The effect of sample pH on AuNPs@PMo$_{12}$ sensing ability for detection of AP was studied (Fig. 9 and S1†). The pH of the AuNPs@PMo$_{12}$ solution (after preparation due to presence of PMo$_{12}$ in as-prepared solution) was 3.0 ± 0.5, and the other pH values were adjusted using NaOH solution. As shown in Fig. S1† and 9, at lower pH (pH $\sim3.0 \pm 0.5$), the SPR peaks show red-shifted in different concentrations. Furthermore, more color change of AuNPs@PMo$_{12}$ from red to blue could be observed in the case of nanosensor at pH 3.0 ± 0.5. Since the pK_a value of H$_3$Mo$_{12}$O$_{40}$ in aqueous solution are 2.4, 4.3, and 5.5,[44] AuNPs@PMo$_{12}$ in pH $\sim 3.0 \pm 0.5$ should exist in nearly negative
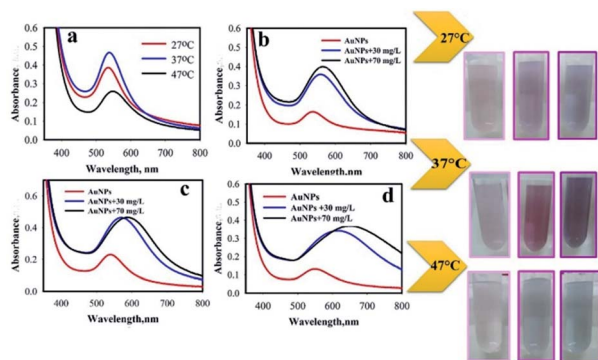

Fig. 6 Effect of reaction temperature on (a) SPR peak of AuNPs@PMo$_{12}$, (b) upon addition of AP ($T = 27 \pm 1$ °C), (c) ($T = 37 \pm 1$ °C), and (d) $T = 47 \pm 1$ °C (pictures show visual color change due to addition of AP solution into AuNPs@PMo$_{12}$ solution (from left to right): AuNPs + 0 mg L^{-1}, AuNPs + 30 mg L^{-1}, and AuNPs + 70 mg L^{-1}), (synthesis condition: intensity = 26 W cm^{-2}, Au : POM ratio (1 : 2)).
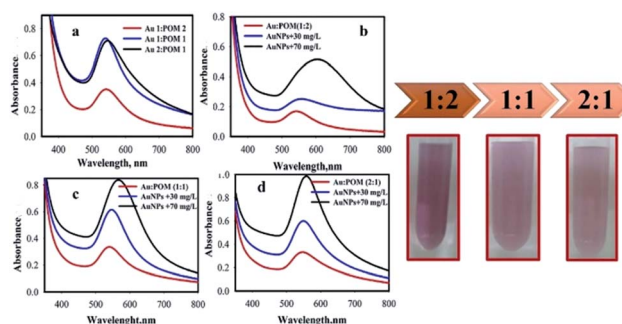

Fig. 8 Effects of different Au : POM ratios on (a) SPR peak of AuNPs@PMo$_{12}$ (b) upon addition of AP solution (Au 1 : POM 2), (c) (Au 1 : POM 1), and (d) (Au 2 : POM 1), (pictures show visual color change of AuNPs@PMo$_{12}$ after addition of AP (30 mg L^{-1}) (synthesis condition: intensity = 26 W cm^{-2}, $T = 37 \pm 1$ °C).
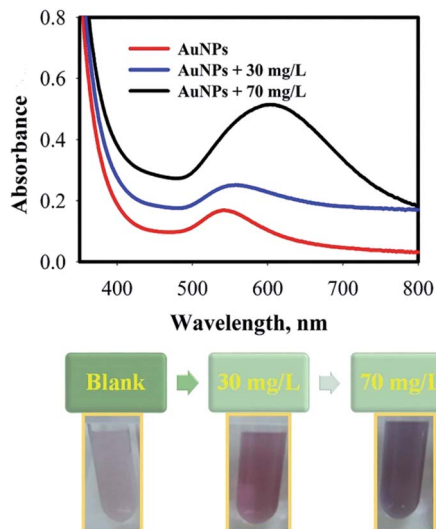
Fig. 9 UV-visible absorption spectra of AuNPs@PMo$_{12}$ upon addition of AP solution at pH 3.0 ± 0.5. (Photographic images: AuNPs + 0 mg L^{-1} (blank), AuNPs + 30 mg L^{-1}, and AuNPs + 70 mg L^{-1}) (synthesis condition: intensity; 26 W cm^{-2}, $T = 37 \pm 1$ °C, Au : POM ratio (1 : 2)).

Fig. 10 (a) UV-visible spectra of AuNPs@PMo$_{12}$ solutions with different concentrations of AP, (b) calibration graphs for the quantification of AP by using AuNPs@PMo$_{12}$ as colorimetric probe, and photographic images of AuNPs@PMo$_{12}$ in concentration range of 1 to 120 mg L^{-1} (concentrations of all AP solution were (from left to right) 0, 1, 3, 6, 10, 15, 20, 30, 50, 70, 100 and 120 mg L^{-1}, respectively).

charge which confirmed with ζ-potential characterization, and the surface charge should be more negative by increasing of pH. Besides, the AP molecule as a weak electrolyte with a pK_a value of 9.5 and both ionized (base) form and non-ionized (acid) form co-exist in the aqueous solution. According to the pH of the aqueous solution, the distribution of an acidic and basic form of AP change.[28]

It was reported that 90% of AP is in the protonated form in pH < 7.0, and in the basic solution proton of phenol group is removed. At pH 11.0, 90% of the deprotonated form of AP exists in the aqueous solution.[28] So, it is suggested that the AP molecule is in the non-ionized form in acidic medium (pH ~3.0 ± 0.5) and the AuNPs aggregation was induced by AP through hydrogen bonding and donor–acceptor electron complexes.[28,45] It is assumed that the generation of donor–acceptor electron complexes occurred between the free electron pair groups like oxygen groups of MoO$_{12}$ onto the surface of AuNPs and the electropositive nitrogen in AP molecule.[28]

In basic media, PMo$_{12}$ is not stable; therefore, it may degrade to some new Mo-based compounds and change the structure of the nano-hybrid. Also, in the basic media repulsion force between the negative charge of AuNPs@PMo$_{12}$ nano-hybrid and deprotonated form of negative charge of AP occurred. So, the aggregation of AuNPs cannot be induced by AP molecules. According to the ESI (Fig. S1†), no significant color change is seen in neutral and basic media. Therefore, pH 3.0 ± 0.5 (natural pH of nanosensor) was selected for AuNPs@PMo$_{12}$-based colorimetric assays of AP.

Colorimetric assay of acetaminophen

To test the analytical performance of AuNPs@PMo$_{12}$, different concentrations of AP were added into individual AuNPs@PMo$_{12}$
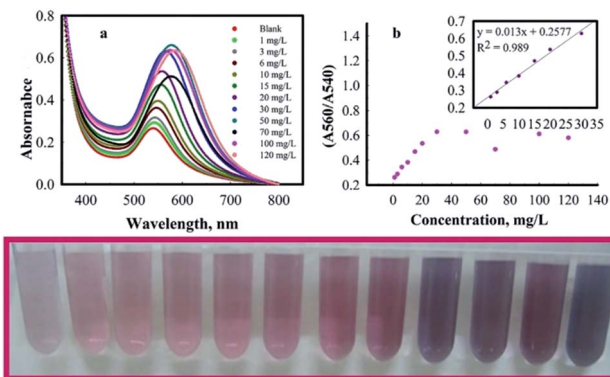
solutions at pH 3.0 ± 0.5. The changes of AuNPs@PMo$_{12}$ dispersions both in terms of the color and the absorbance spectra are recorded and shown in Fig. 10. These results indicate that linear correlation existed between intensity ratio ($A_{560/540}$) versus concentration of AP, over the range of 1–30 mg L^{-1} with regression equation of $y = 0.0242x + 0.4798$ (0.989). The absorbance ratio (A_{560}/A_{540}) increased with increasing of AP concentration. As a result, the limit of detection (LOD) was found to be 0.42 mg L^{-1}.

Quantitative determination of acetaminophen by smartphone as a chemical detector

The extraordinary development of smartphones and tablets has made a great opportunity for researchers to develop their methods by using smartphones as a chemical detector.[46] These highly reliable portable devices which have a digital camera and internal microprocessor for image processing, reduce using external computers and expensive devices.[46] In this work, to obtain the calibration curve by analyzing the average RGB (red, green, and blue) value, the pictures of different concentrations of AP samples were taken. To verify the reliability of the smartphone as a chemical detector, we used two methods for analyzing the color changes. The RGB values were obtained by eyedropper function in Microsoft Office PowerPoint 2016 software and ImageJ software. Quantitative determination was made by transforming the RGB value to AP concentration. As shown in the Fig. 11, the trend of RGB values of ImageJ is consistent with eyedropper. The linear range for AP values was observed from 3 to 50 mg L^{-1} with regression equation of $y = -1.6208x - 17.642$ (0.9886).

The quantitative result which was generated automatically by the eyedropper function in the PowerPoint 2016 software and ImageJ, was matched by the corresponding sample concentration in the colorimetric curve. As shown in the graphs, RGB values indicated linear behavior which is consistent with our previous results. This method is cost-efficient and more
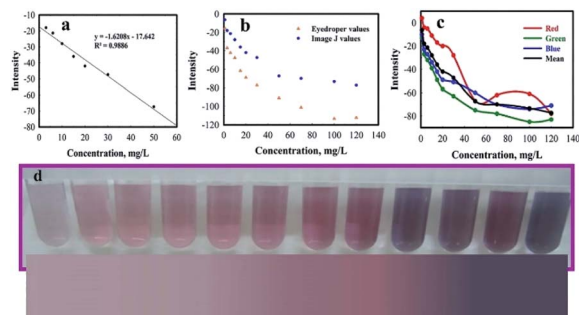
Fig. 11 (a) Calibration curve of ImageJ response to different concentration of AP, (b) quantifying the colorimetric results with two different colorimetric methods, (c) comparison of the response of RGB and mean with different concentrations of AP (1–120 mg L^{-1}), (d) the corresponding RGB values for the samples (concentrations of all AP solution were (from left to right) 0, 1, 3, 6, 10, 15, 20, 30, 50, 70, 100 and 120 mg L^{-1}, respectively), and its corresponding location in the colorimetric curve.

practical compared to the methods using expensive instruments with complicated sample preparation.

Selectivity of AuNPs@PMo$_{12}$ for acetaminophen

The specificity of the AuNPs@PMo$_{12}$ nano-hybrid was studied by comparing the colour change of solution upon the separate addition of the drugs (acetaminophen (AP), methadone (MTD), methylphenidate (MEPS), tramadol (TRA), ibuprofen (IBP), aspirin (ASA), codeine (COD), and diclofenac (DIC)). These drugs were used to test the selectivity of the system for acetaminophen (C$_8$H$_9$NO$_2$), because several of these drugs – MEPS, TRA, and MTD – are commonly used by people in conjunction with other over-the-counter drugs to achieve similar analgesic effects. In this test, acetaminophen, AP (C$_8$H$_9$NO$_2$) with concentration of 0.46 mmol L^{-1} was used. Methadone, MTD (C$_{21}$H$_{27}$NO), methylphenidate, MEPS (C$_{14}$H$_{19}$NO$_2$), tramadol, TRA (C$_{16}$H$_{25}$NO$_2$), ibuprofen, IBP (C$_{13}$H$_{18}$O$_2$), aspirin, ASA (C$_9$H$_8$O$_4$), diclofenac, DIC (C$_{14}$H$_{11}$Cl$_2$NO$_2$), and codeine, COD (C$_{18}$H$_{21}$NO$_3$) with a concentration of 0.92 mmol L^{-1} were added into AuNPs@PMo$_{12}$ solution separately and in combination with AP solution. As seen in Fig. 12a, after the addition of AP, a significant color change occurred where the maximum shifts from 540 nm to 600 nm. The chemical structure of other drugs are shown in Fig. S2.† It is found that the drug with a group (–N) forms hydrogen bonding and donor–acceptor electron complexes into AuNPs@PMo$_{12}$ surface. Among these drugs AP is the only one with a functional group (–NH) from an amide bond in molecular structure and it is our hypothesis that, due to less steric hindrance around this group, it shows more interaction by AuNPs@PMo$_{12}$ surface. DIC shows a different color change compared to the other drugs, changing to orange-yellow. Importantly, the drugs which have no (–N) groups do not appear to interact with the AuNPs@PMo$_{12}$ surface, so drugs such as ASA and IBP clearly produce almost no alteration of the AuNPs@PMo$_{12}$ spectrum, as shown in Fig. 12a.

Fig. 12b shows the UV-vis spectra of AuNPs@PMo$_{12}$ solutions for the selective detection of AP from a combination of
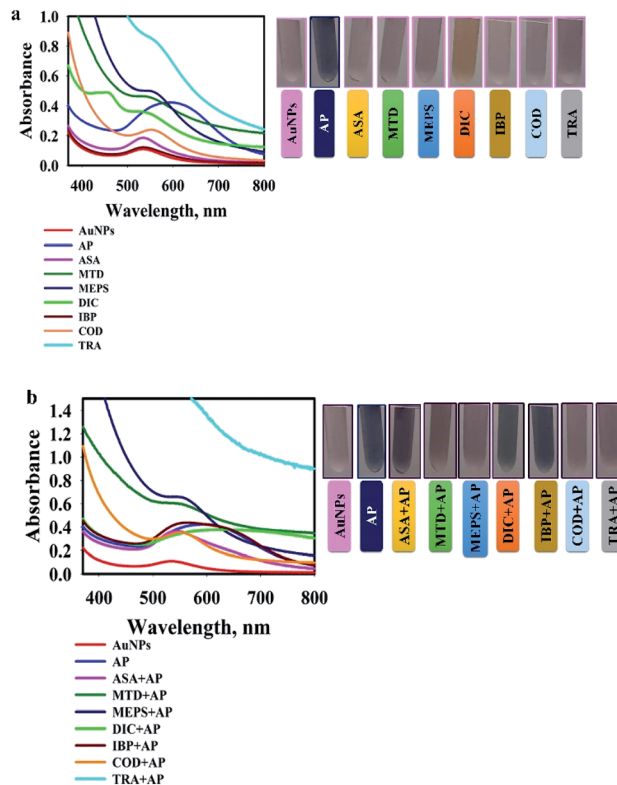

Fig. 12 (a) UV-visible spectra of AuNPs@PMo$_{12}$ solutions with different drugs, where the concentration of AP = 0.46 mmol L^{-1}, and all other drugs = 0.92 mmol L^{-1}, and related photographic images; (b) UV-visible spectra of AuNPs@PMo$_{12}$ solutions incubated with different drugs + AP (together), where the concentration of AP = 0.46 mmol L^{-1}, and all other drugs = 0.92 mmol L^{-1}, and related photographic images.

different drugs. In these experiments, the UV-vis spectra of AuNPs@PMo$_{12}$ was measured when AP (at a concentration of 0.46 mmol L^{-1}) was added with other commercially available drugs (at a concentration of 0.92 mmol L^{-1}). The photographs illustrate that for the naked eye detection, the selective detection is only evident for the four of the seven drugs that were evaluated and it is clear that the more subtle colour changes observed for combinations of ASA + AP, DIC + AP and IBP + AP require further analytical confirmation. The absorption profiles from the UV-vis spectra confirm the selective and specific interaction of only AP molecules with the nanosensor and clear differences between all the drug combinations.

Sensing mechanism

To verify the mechanism of AuNPs aggregation in the presence of Ap, the following experiment was carried out: after the reaction nanosensor with AP, the final product was centrifuged and washed many times to purify and separate from the synthesis media. The purified AuNPs were dispersed in deionized water, which was tested with an AP solution (0.9 mL of nanosensor solution +0.9 mL of AP solution with 70 mg L^{-1}) (solution A). After adding AP solution, there was no change in color of the solution and UV-vis spectrum of AuNPs@PMo$_{12}$
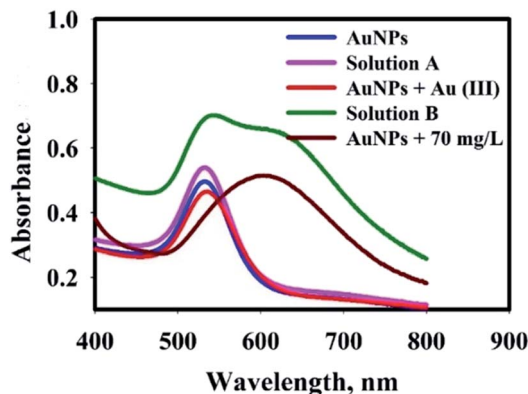
Fig. 13 UV-visible spectra of AuNPs@PMo$_{12}$ solutions in a different condition to determine mechanism of AP detection.

Scheme 2 Illustration of the detection mechanism of AP using AuNP@PMo$_{12}$ nano-hybrid.

(Fig. 13). After that, 0.1 mL of Au(III) solution (1 mM) was added to solution A (solution B). Results exhibited a change in color and UV-vis spectrum by the addition of the Au ions solution.
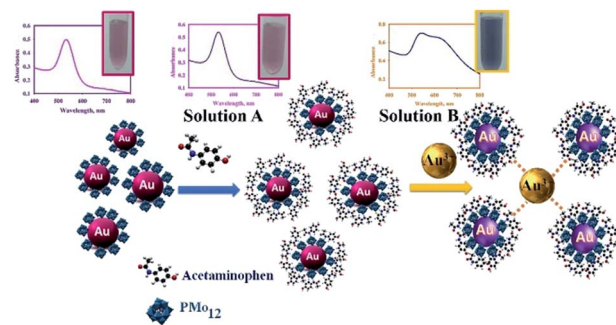
In our research work, there are some important observation which can be listed as follows: (1) after synthesis process, the solution of AuNPs@PMo$_{12}$ showed red color due to its strong surface plasmon resonance at *ca.* 540 nm, and the addition of AP solution led to color change which was due to interparticle crosslinking and the aggregation of AuNPs; (2) In presence of Au(III) ions, AuNPs@PMo$_{12}$ aggregated after addition of the AP molecules.

So, the following mechanism is assumed whereby AP is able to ionize in aqueous solution as follows (eqn (11)):

$$C_8H_9NO_2 \Leftrightarrow C_8H_8NO_2^- + H^+ \qquad (11)$$
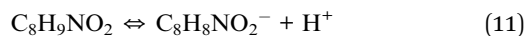
The pK_a for ionization of AP molecules shown by eqn (11) is reported to be 9.5.[29] The pH of nanosensor is 3.0 ± 0.5. Thus, at this pH, AP mainly exists in the form shown by the left-hand side of eqn (11). According to the zeta potential results, the surface of AuNPs@PMo$_{12}$ was nearly negative, but the ζ-potential was not sufficiently high. In addition, the AP molecules are in a non-ionized form in the pH of the nanosensor (pH ~3.0 ± 0.5). So, it is suggested that the electrostatic interaction is not a predominant factor in binding between AuNPs@PMo$_{12}$ and AP molecules. The target analyte (AP) with a functional group (–NH) forms hydrogen bonding and donor–acceptor electron complexes into AuNPs@PMo$_{12}$ surface. Besides, AP molecules strongly induced the AuNPs@PMo$_{12}$ aggregation in the presence of Au(III) ions. It is proposed that Au(III) can interact with –OH groups of AP molecules *via* donor–acceptor electron complex which causes the interparticle cross linking between AuNPs and then change in color (Fig. 13 and Scheme 2). Therefore, AP can rapidly induce the aggregation of AuNPs in the presence of unreacted Au(III) ions which exist in nanosensor media. It is also possible that H-bonding between AP molecules adsorbed to neighbor AuNPs@PMo$_{12}$ took place.

As mentioned, PMo$_{12}$ was used as a capping and reducing agent for the synthesis of AuNPs without further modifications. In order to examine the change in the average size and
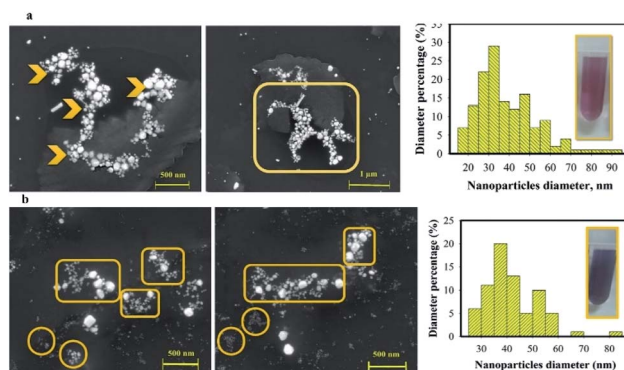

Fig. 14 (a) SEM image of AuNPs@PMo$_{12}$ nano-hybrids after the addition of AP (30 mg L^{-1}). (b) SEM image of AuNPs@PMo$_{12}$ nano-hybrids after the addition of AP (70 mg L^{-1}). (Marked area shows aggregated particles).

morphology of AuNPs, we considered the AP-induced aggregation of AuNPs@PMo$_{12}$ by SEM. As shown in Fig. 14, the average size of AuNPs nanoparticles increased from 20 nm to 38 nm and 42 nm upon addition of AP with a concentration of 30 mg L^{-1} and 70 mg L^{-1}, respectively. The morphology of AuNPs@PMo$_{12}$ was influenced by the addition of AP. AP molecules lead to the inter-particle distance reduction of AuNPs (Fig. 14).

This colorimetric strategy exhibited high sensitivity and excellent selectivity for the detection of AP because of the high efficiency and great specificity of nanostructured supramolecular chemistry. AFM analysis also shows the aggregation of
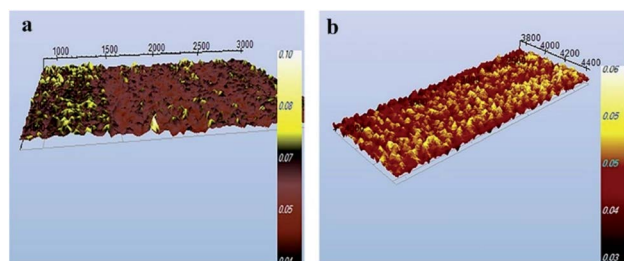

Fig. 15 AFM image of AuNPs@PMo$_{12}$ nano-hybrids (a) before and (b) after the addition of AP (70 mg L^{-1}) (synthesis condition; intensity; 26 W cm^{-2}, $T = 37 \pm 1$ °C, Au : POM ratio (1 : 2)).

Table 1 Determination and comparison of serum levels of AST and ALT at two and five hours after AP administration based on nanosensor results

		Toxic group, $N = 73$	Suspicious group, $N = 22$	Non-toxic group, $N = 5$	P-value[a]
Serum AST level (mg L^{-1})	After 2 h	106.22 ± 0.78	100.15 ± 0.03	108.7 ± 0.78	<0.001
	After 5 h	274.49 ± 4.6	173.17 ± 0.1	134.85 ± 0.48	<0.001
	P value[b]	<0.001	<0.001	<0.001	
Serum ALT level (mg L^{-1})	After 2 h	32.54 ± 0.42	32.76 ± 0.81	32.68 ± 0.38	>0.05
	After 5 h	156.5 ± 5.24	93.91 ± 1.08	44.54 ± 1.57	<0.001
	P value[b]	<0.001	<0.001	<0.001	

[a] Kruskal Wallis test was used for comparison between the 3 groups. [b] Wilcoxon Singed Ranks test was used to examine intra-group changes.

AuNPs@PMo$_{12}$ nano-hybrids after addition of AP in nanosensor media (Fig. 15). Scheme 2 indicates the detection mechanism of AP in the presence of AuNPs@PMo$_{12}$ nano-hybrid and Au(III) ions.

Determination of acetaminophen in mice serum samples with AuNPs@PMo$_{12}$ nanosensor

Mean serum AST‡ and ALT§ levels were measured two hours and five hours after drug administration. As shown in Table 1, the results obtained in this study based on the nanosensor showed that 73 mice had levels above 100 μg mL^{-1} (toxic level), 22 mice had levels between 25-100 μg mL^{-1} (suspicious), and 5 mice had levels less than 25 μg mL^{-1} (non-toxic level).

According to the results, changes in both AST and ALT enzymes showed a significant increase at the fifth hour after AP administration compared to the second hour ($p < 0.001$). Spearman's correlation coefficient between nanosensor results and serum AST enzyme level two hours after drug administration was $r = 0.407$ and $p < 0.001$ and five hours after drug administration was $r = 0.775$ and $p < 0.001$, indicating very high agreement between the two tests.

Spearman's correlation coefficient between nanosensor results and serum ALT enzyme level two hours after drug administration was $r = 0.292$ and $p = 0.003$ and five hours after drug administration was $r = 0.775$ and $p < 0.001$, indicating very high agreement between the two tests, especially with the results 5 hours after drug administration. The accuracy of the nanosensor was discussed in the ESI† (see "Diagnostic accuracy of the nanosensor", Fig. S2 and S3 in ESI†).

Conclusions

We have prepared a rapid, simple, low cost and highly specific nanosensor for the quantitative determination of acetamphetamine in blood serum samples. The colorimetric nanoprobes are polyoxometalate-stabilized nanoparticles, AuNP@PMo$_{12}$ which are synthesised using a rapid, facile and eco-friendly sonochemical synthesis. The A_{600}/A_{540nm} values of AuNP@PMo$_{12}$ nano-hybrid biosensor indicated a linear relationship with a concentration range of AP (1–30 mg L^{-1}). Importantly, both the qualitative and quantitative

determination of AP were investigated, and our method demonstrated the limit of detection to be as low as 0.42 mg L^{-1}. These results showed that this nanosensing set-up could potentially be used in a clinical setting for the real-time point-of-care detection of AP with accuracy, convenience, and efficiency, even in the presence of other pharmaceuticals, in this instance methadone, methylphenidate, and tramadol. Future work will involve the practical application of this set-up by integrating mobile phone devices and the appropriate applications to detect a range of AP in more complex media, e.g. other buffers, cell culture media, patient blood serum, and so forth.

Conflicts of interest

There are no conflicts to declare.

Acknowledgements

References

1 E. Yoon, A. Babar, M. Choudhary, M. Kutner and N. Pyrsopoulos, *J. clin. transl. hepatol.*, 2016, **4**, 131–142.
2 C. M. Herndon and D. M. Dankenbring, *Journal of Pain and Palliative Care Pharmacotherapy*, 2014, **28**, 109–116.
3 R. Clark, J. E. Fisher, I. S. Sketris and G. M. Johnston, *BMC Clin. Pharmacol.*, 2012, **12**, 11.
4 G. Corcoran, W. Racz, C. Smith and J. Mitchell, *J. Pharmacol. Exp. Ther.*, 1985, **232**, 864–872.
5 S. H. Rhyee, *Academic Emergency Medicine*, 2013, **20**, 1070–1071.
6 G. Burgot, F. Auffret and J.-L. Burgot, *Anal. Chim. Acta*, 1997, **343**, 125–128.
7 S. Ravisankar, M. Vasudevan, M. Gandhimathi and B. Suresh, *Talanta*, 1998, **46**, 1577–1581.
8 A. B. Moreira, H. P. Oliveira, T. D. Atvars, I. L. Dias, G. O. Neto, E. A. Zagatto and L. T. Kubota, *Anal. Chim. Acta*, 2005, **539**, 257–261.

‡ Aspartate aminotransferase.
§ Alanine transaminase.

9 S. Zhao, W. Bai, H. Yuan and D. Xiao, *Anal. Chim. Acta*, 2006, **559**, 195–199.

10 A. Cernat, M. Tertiș, R. Săndulescu, F. Bedioui, A. Cristea and C. Cristea, *Anal. Chim. Acta*, 2015, **886**, 16–28.

11 L. Tang and J. Li, *ACS Sens*, 2017, **2**(7), 857–875.

12 Y. Guo and W. Zhao, *Coord. Chem. Rev.*, 2019, **387**, 249–261.

13 H. G. T. Ly, G. Absillis, R. Janssens, P. Proost and T. N. Parac-Vogt, *Angew. Chem., Int. Ed.*, 2015, **54**, 7391–7394.

14 A. González, N. Gálvez, M. Clemente-León and J. M. Dominguez-Vera, *Chem. Comm.*, 2015, **51**, 10119–10122.

15 D.-F. Chai, Z. Ma, H. Yan, Y. Qiu, H. Liu, H.-D. Guo and G.-G. Gao, *RSC Adv.*, 2015, **5**, 78771–78779.

16 A. Troupis, A. Hiskia and E. Papaconstantinou, *Angew. Chem., Int. Ed.*, 2002, **41**, 1911–1914.

17 Y. Wang and I. A. Weinstock, *Chem. Soc. Rev.*, 2012, **41**, 7479–7496.

18 S. G. Mitchell and J. M. de la Fuente, *J. Mater. Chem.*, 2012, **22**, 18091–18100.

19 Z. Lang, I. M. Gabas, X. López, A. Clotet, J. M. de la Fuente, S. G. Mitchell and J. M. Poblet, *New J. Chem.*, 2016, **40**, 1029–1038.

20 G. Zhang, B. Keita, R. N. Biboum, F. Miserque, P. Berthet, A. Dolbecq, P. Mialane, L. Catala and L. Nadjo, *J. Mater. Chem.*, 2009, **19**, 8639–8644.

21 R. Liu, S. Li, G. Zhang, A. Dolbecq, P. Mialane and B. Keita, *J. Cluster Sci.*, 2014, **25**, 711–740.

22 L. Suo, W. Gao, Y. Du, R. Wang, L. Wu and L. Bi, *New J. Chem.*, 2016, **40**, 985–993.

23 A. Ayati, A. Ahmadpour, F. F. Bamoharram, M. M. Heravi and H. Rashidi, *Chin. J. Catal.*, 2011, **32**, 978–982.

24 H. Xu and K. S. Suslick, *ACS Nano*, 2010, **4**, 3209–3214.

25 T. Rohani Bastami and M. H. Entezari, *Ultrason. Sonochem.*, 2012, **19**, 830–840.

26 K. Okitsu, M. Ashokkumar and F. Grieser, *J. Phys. Chem.*, 2005, **109**(44), 20673–20675.

27 S. Anandan, F. Grieser and M. Ashokkumar, *J. Phys. Chem. C*, 2008, **112**(39), 15102–15105.

28 V. Bernal, A. Erto, L. Giraldo and J. C. Moreno-Piraján, *Molecules*, 2017, **22**, 1032–1046.

29 A. Ayati, A. Ahmadpour, F. F. Bamoharram, M. M. Heravi and M. Sillanpää, *Gold Bullet*, 2012, **45**, 145–151.

30 L. L. Mazaleuskaya, K. Sangkuhl, C. F. Thorn, G. A. FitzGerald, R. B. Altman and T. E. Klein, *PharmGKB*, 2015, **25**, 416–426.

31 T. Rohani Bastami and M. H. Entezari, *Ultrason. Sonochem.*, 2012, **19**, 560–569.

32 J. Chen, S. Liu, W. Feng, G. Zhang and F. Yang, *Phys. Chem. Chem. Phys.*, 2013, **15**, 5664–5669.

33 E. Papaconstantinou, *Chem. Soc. Rev.*, 1989, **16**, 1–31.

34 E. Papaconstantinou and A. Hiskia, in *Polyoxometalate Molecular Science*, ed. J. J. Borrás-Almenar, E. Coronado, A. Müller and M. Pope, Springer Netherlands, Dordrecht, 2003, p. 381.

35 Z. Mohammadi and M. H. Entezari, *Ultrason. Sonochem.*, 2018, **44**, 1–13.

36 Z. Li, A. Friedrich and A. Taubert, *J. Mater. Chem.*, 2008, **18**, 1008–1014.

37 J. Xu, T. Zhao, Z. Liang and L. Zhu, *Chem. Mater.*, 2008, **20**, 1688–1690.

38 S. Khadempir, A. Ahmadpour, M. T. Hamed Mosavian, N. Ashraf, F. F. Bamoharram, S. G. Mitchell and J. M. de la Fuente, *RSC Adv.*, 2015, **5**, 24319–24326.

39 S. Khadempir, A. Ahmadpour, M. T. Hamed Mosavian, N. Ashraf, F. F. Bamoharram, R. Fernández-Pacheco, J. M. de la Fuente and S. G. Mitchell, *RSC Adv.*, 2016, **6**, 5359–5366.

40 T. Mazari, C. R. Marchal, S. Hocine, N. Salhi and C. Rabia, *J. Nat. Gas Chem.*, 2010, **19**, 54–60.

41 X.-j. Wang, X. Li and S. Yang, *Energy Fuels*, 2009, **23**, 2684.

42 T. Rohani Bastami and M. H. Entezari, *Mater. Res. Bull.*, 2013, **48**, 3149–3156.

43 S. K. Laliwala, V. N. Mehta, J. V. Rohit and S. K. Kailasa, *Sens. Actuators, B*, 2014, **197**, 254–263.

44 E. A. Nagul, I. D. McKelvie, P. Worsfold and S. D. Kolev, *Anal. Chim. Acta*, 2015, **890**, 60–82.

45 L. F. Prescott, *Br. J. Clin. Pharmacol.*, 1980, **10**(suppl. 2), 291S.

46 J. Du, H. Ge, Q. Gu, H. Du, J. Fan and X. Peng, *Nanoscale*, 2017, **9**, 19139–19144.